Geophysical Research Letters

RESEARCH LETTER
10.1029/2023GL104413

State-Dependence of the Equilibrium Climate Sensitivity in a Clear-Sky GCM

Matthew Henry[1], Geoffrey K. Vallis[1], Nicholas J. Lutsko[2], Jacob T. Seeley[3], and Brett A. McKim[1,4]

[1]Department of Mathematics, University of Exeter, Exeter, UK, [2]Scripps Institution of Oceanography, La Jolla, CA, USA, [3]Department of Earth and Planetary Sciences, Harvard University, Cambridge, MA, USA, [4]LMD/IPSL, CNRS, Sorbonne Université, Paris, France

Key Points:

- Climate sensitivity peaks around 310 K in a variety of climate models, ranging from idealized single column models to comprehensive models
- We use a clear-sky GCM to bridge the gap between comprehensive models and single column models for which we have a theory for this peak
- At high CO_2, changes in atmospheric circulation cause a moistening of the subtropical regions and increase the climate sensitivity

Supporting Information:

Supporting Information may be found in the online version of this article.

Correspondence to:

M. Henry,
matthew.jo.henry@gmail.com

Citation:

Henry, M., Vallis, G. K., Lutsko, N. J., Seeley, J. T., & McKim, B. A. (2023). State-dependence of the equilibrium climate sensitivity in a clear-sky GCM. *Geophysical Research Letters*, *50*, e2023GL104413. https://doi.org/10.1029/2023GL104413

Received 4 MAY 2023
Accepted 5 NOV 2023

Abstract The climate sensitivity peaks around 310 K in a wide variety of climate models, ranging from idealized single column models to fully comprehensive climate models. Here, we increase CO_2 using a clear-sky three-dimensional atmospheric model with a radiation scheme which maintains accuracy for high CO_2 and temperature levels. In contrast, the Equilibrium Climate Sensitivity (ECS) of our model plateaus around 310 K. We show that this is due to the moistening of the subtropical regions caused by a slowdown in atmospheric circulation, which increases the ECS at very high CO_2 values. When relative humidity is fixed, the ECS peak is consistent with single column model results. This work does not rule out that clouds or other complex processes impact the ECS in comprehensive climate models. Though the changes in CO_2 here are extreme, this study underlines the importance of changes in atmospheric circulation and relative humidity in quantitative assessments of climate sensitivity.

Plain Language Summary From simple single column models to fully comprehensive three-dimensional climate models, when we increase CO_2 to very high levels, we find a peak in the temperature increase per doubling of CO_2 at around 310 K. While we understand why this happens in simple models, we lack an understanding for fully comprehensive climate models. Our study uses an intermediate complexity three-dimensional climate model to bridge this gap. We find that the peak in climate sensitivity is not as pronounced as in other studies. We show that this is due to large changes in the atmospheric circulation which causes a moistening of the subtropics and an increase in the climate sensitivity.

1. Introduction

Equilibrium climate sensitivity (ECS) is defined as the amount by which surface temperature changes after a doubling of CO_2 and when equilibrium has been reached. That equilibrium is somewhat ill-defined, and there is both paleoclimate (Anagnostou et al., 2020) and climate model evidence (Bloch-Johnson et al., 2021) that the ECS is state-dependent and increases at higher temperature. Moreover, Bloch-Johnson et al. (2021) found that, for almost all models from the Sixth Coupled Model Intercomparison Project, the clear-sky longwave feedback is less stabilizing at high temperatures, whereas there is no such agreement for the other components of the climate feedback. This can be understood to be a consequence of the closing of the atmospheric water vapor window (Koll & Cronin, 2018; Koll et al., 2023).

By systematically increasing either the solar constant or greenhouse gas concentrations, a peak in ECS has been found around 310 K in a variety of climate models spanning the climate model hierarchy (e.g., Leconte et al., 2013; Meraner et al., 2013; Popp et al., 2016; Romps, 2020; Russell et al., 2013; Wolf & Toon, 2015; Wolf et al., 2018). However, Kluft et al. (2021) show that an out-of-bounds use of comprehensive climate model radiation schemes can lead to an erroneously large peak in ECS, and that may explain the much larger peaks in ECS in comprehensive climate models compared to the single column calculations with more accurate radiation schemes by Kluft et al. (2021) and Seeley and Jeevanjee (2021). Both studies show a peak in ECS of around 5 K at approximately 310 K when CO_2 is increased. Seeley and Jeevanjee (2021) show that the peak in ECS is due to a competition between the closing of the water vapor window and the opening of the CO_2 radiator fins, but this explanation only applies to a world warmed by increasing CO_2, rather than increasing the solar constant, and only to an atmosphere in radiative-convective equilibrium.

The single column calculations by Kluft et al. (2021) and Seeley and Jeevanjee (2021) are based on a single column model with constant relative humidity. Zhang et al. (2020) analyze comprehensive climate model simulations and show the role of having a constant distribution in column relative humidity in producing a constant clear-sky longwave feedback. Bourdin et al. (2021) use a radiative-convective single column model to show that the vertical structure of relative humidity also affects the clear-sky longwave feedback as it determines the emission temperature which is felt at the top of the atmosphere. This previous work suggests that both the climatological relative humidity and any changes to the relative humidity distribution will play an important role in shaping the clear-sky longwave feedback.

In this work, we analyze a range of climates using a clear-sky configuration of Isca (Vallis et al., 2018), with a comprehensive radiation scheme that maintains good accuracy for atmospheres with up to 10% CO_2 by volume (i.e., 100,000 ppm) and 500 K. This provides a connection between the single column model with line-by-line radiation computation (Kluft et al., 2021; Seeley & Jeevanjee, 2021) and more comprehensive three-dimensional GCMs. In particular, we show that increases in subtropical relative humidity caused by a slowdown in atmospheric circulation destabilize the clear-sky longwave feedback and increase the ECS at high CO_2. It is important to note that our work does not rule out the possibility that clouds and other complex processes may impact the ECS. We simply suggest that a more basic mechanism, one which should be in all GCMs, is at play. We first describe the model and experiments. Second, we describe the changes in the atmospheric energy transport and relative humidity, then analyze how changes in relative humidity affect the radiative feedback. Finally, we confirm our understanding through a latitudinal decomposition of the relative humidity and feedback.

2. Model and Experimental Description

We increase CO_2 in a clear-sky aquaplanet configuration of the Isca climate modeling framework (Vallis et al., 2018), here configured with no sea ice, a slab ocean boundary condition, no land or topography, a hydrology cycle but no clouds, and annual-mean insolation. We use the comprehensive SOCRATES radiation scheme for infra-red and solar radiation (Manners et al., 2017; Thomson & Vallis, 2019), and this maintains good accuracy for up to 10% CO_2 and 500 K. The surface albedo is set uniformly to 0.15. Simulations are run at spectral T42 resolution, which corresponds to approximately 2.8 degrees resolution at the equator. Convection is calculated using a simplified Betts-Miller convection scheme (Frierson, 2007). Large scale condensation is parameterized such that relative humidity does not exceed one, and condensed water immediately returns to the surface. Popp et al. (2016) found that removing stratospheric ozone may affect upper atmospheric levels of moisture but makes no substantial difference to the surface climate, and Wolf and Toon (2015) and Leconte et al. (2013) do not include ozone in their simulations. We hence choose not to include stratospheric ozone.

We perform experiments in which CO_2 concentration is variously set to 300, 600, 1,200, 2,400, 4,800, 9,600, $9{,}600\sqrt{2}$, 19,200, $19{,}200\sqrt{2}$, 38,400, $38{,}400\sqrt{2}$, 76,800, and 76,800 ppm $\sqrt{2} \approx 110{,}000$ ppm for 100 months each successively. We include simulations with $\sqrt{2}$ increases in the concentration of CO_2 in order to give a more uniform resolution of ECS values around the 310 K peak in global-mean surface temperature (GMST). In what follows, the CO_2 concentration will be expressed as 300 ppm $\times 2^i$ with $i = [0, 1, 2, 3, 4, 5, 5.5, 6, 6.5, 7, 7.5, 8, 8.5]$. The simulations all reach an equilibrium after approximately 30 months as the net TOA radiation reaches zero and the surface temperature stabilizes. The values shown in the manuscript are the time-mean of the last 50 months of the simulation. Figure 1 shows the ECS for each increase in CO_2. To compare temperature increases across the different increases in CO_2 concentration, we normalize the temperature increase by the fractional increase in CO_2 concentration, as the forcing from CO_2, and hence the temperature increase, depend on the logarithm of CO_2 concentration. The experiments are summarized in Table 1 along with their forcing (F). Details on the calculation of the forcing F are given in Section 4. The ECS plateaus at around 305 K in GMST, with a mild maximum at 311 K (Figure 1).

Figure S1 in Supporting Information S1 shows the temperature and radiative temperature tendencies of two versions of Isca in single column mode: one with the radiation scheme used in the standard three-dimensional version of the GCM (17 bands) used for the simulations described above and one with a high resolution radiation scheme (350 bands). The radiative tendencies quantify how each component (radiation, convection, dynamics, etc.) of the climate model affects the temperature at a given location and should sum to zero when the simulation reaches equilibrium. Given the close similarity between the two versions of the single column model, we are

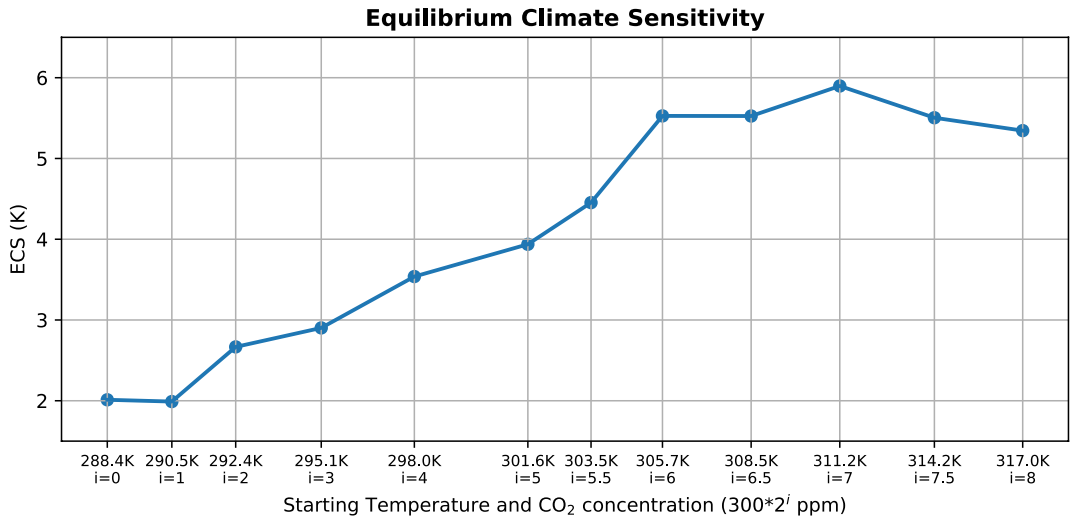

Figure 1. Equilibrium Climate Sensitivity for the suite of clear-sky GCM simulations. The CO_2 concentration is set to 300 ppm × 2^i.

confident in the validity of the radiation scheme used in the full GCM (i.e., the 17 band scheme). We thus avoid the problem of an out-of-bounds use of a GCM radiation scheme, which can lead to an erroneously large peak in ECS, as was found in other comprehensive GCMs (Kluft et al., 2021).

3. Atmospheric Energy Transport and Relative Humidity Changes

Figure 2 shows the relative humidity, atmospheric energy transport, streamfunction, and atmospheric temperature for the 300, 78,600, and 115,200 ppm simulations. The total atmospheric energy transport is calculated using the vertical integral of the net energy fluxes into the atmosphere, and the moist component is calculated using the integral of evaporation minus precipitation times the latent heat of vaporization. The latitudinal gradients of C_pT_S and Lq are shown in Figure S2 in Supporting Information S1, where C_p is the heat capacity of air at constant pressure, T_S is the surface temperature, L is the latent heat of vapourization, and q is the near-surface specific humidity. In the extratropics, the decrease of the latitudinal gradient of C_pT_S and increase of that of Lq are consistent with Figures 2d–2f.

Table 1
Summary of Idealized GCM Experiments

Index i	CO_2 concentration (ppm)	ECS (K)	F (W/m^2)	T_s (K)
0	300	2.0	4.8	288.4
1	600	2.0	5.1	290.5
2	1,200	2.7	5.6	292.4
3	2,400	2.9	6.3	295.1
4	4,800	3.5	7.2	298.0
5	9,600	3.9	8.1	301.6
5.5	13,576	4.5	8.7	303.5
6	19,200	5.5	9.4	305.7
6.5	27,153	5.5	10.1	308.5
7	38,400	5.9	10.8	311.2
7.5	54,306	5.5	11.4	314.2
8	76,800	5.3	11.9	317.0
8.5	108,612			322.3

Note. The Equilibrium Climate Sensitivity (ECS) and the forcing (F) are normalized by the fractional increase in CO_2 concentration, as the forcing from CO_2 and hence the temperature increase depend on the logarithm of CO_2 concentration.

The tropical tropopause height (between 30 degrees North and South) can be estimated by where the radiative cooling rate first goes to zero (Seeley et al., 2019). In the tropics where the atmosphere is in radiative-convective equilibrium, we can equally use the convective criterion, whereby the tropopause is set to where the convective temperature tendency goes below 0.01 K/day. There is a slight difference due to the presence of atmospheric energy export, but this does not meaningfully affect the results and we thus treat them as equivalent. The tropopause is also commonly computed using a 2 K/km lapse rate threshold. Both tropopause calculations are shown in the temperature and streamfunction panels. Figure S3 in Supporting Information S1 shows the lapse rate and convective tropopause pressure and temperature for all simulations. As expected the tropopause goes up in height for all latitudes, but its temperature decreases in the tropics and increases in the extratropics using the 2 K/km lapse rate threshold (Figure S3 in Supporting Information S1), but stays roughly constant when using the convective criterion. The choice of the 2 K/km threshold value works for present-day Earth but should not be expected to apply quantitatively to these idealized very high CO_2 atmospheres. That the fixed tropopause temperature hypothesis does not fully hold in the tropics is expected as that hypothesis assumes

10.1029/2023GL104413

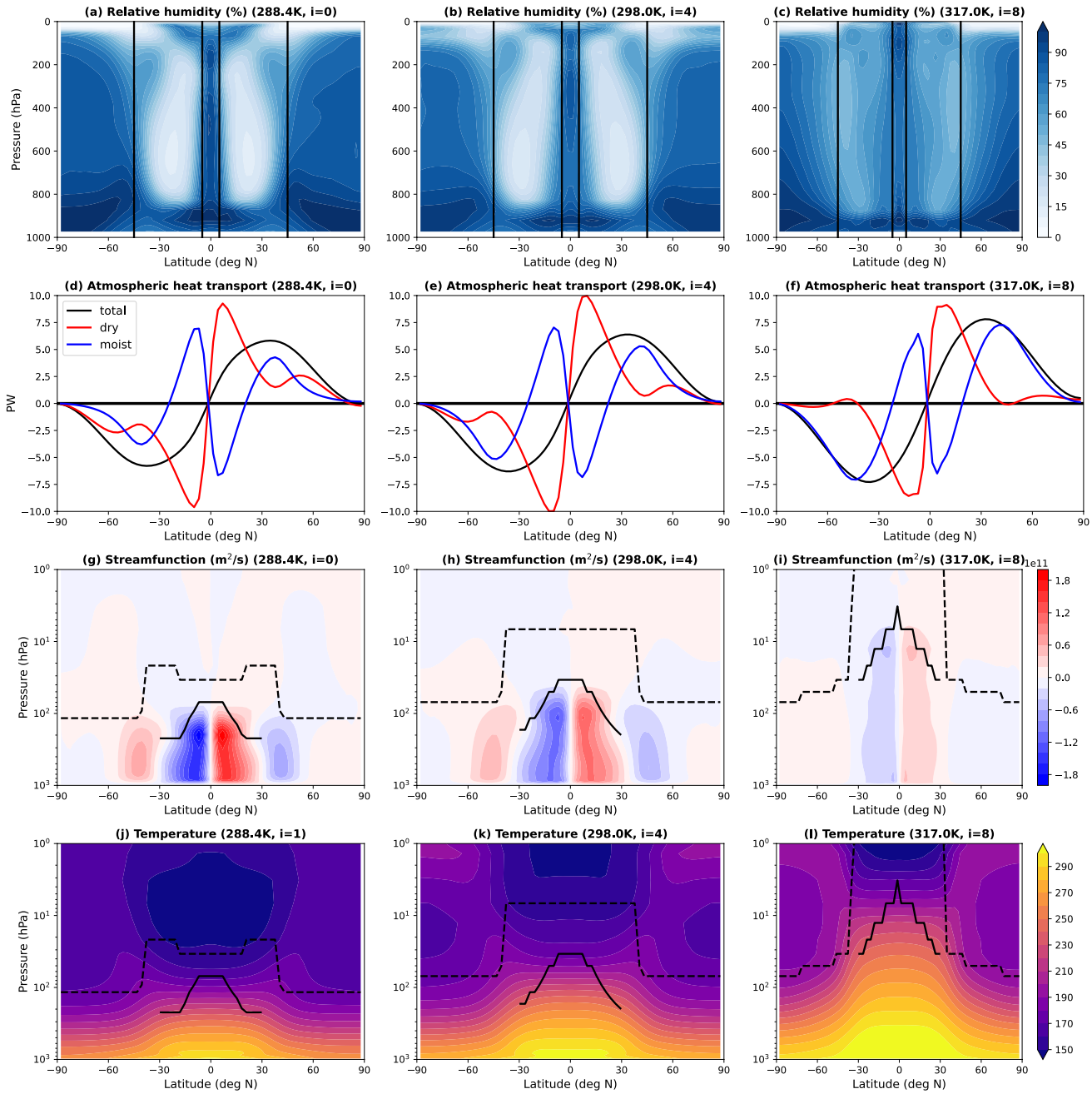

Figure 2. Relative humidity (a–c), atmospheric energy transport (d–f), streamfunction (g–i), and temperature (j–l) for the 300 ppm (a, d, g, j), 36,400 ppm (b, e, h, k), and 115,200 ppm (c, f, i, l) simulations. Note that the *y*-axis in panels (g)–(l) are in log scale. The solid black line in panels (g)–(l) is an estimation of the tropical tropopause using a convective criterion. The dashed black line in panels (g)–(l) is the thermal tropopause, defined by the height at which the lapse rate goes below 2 K/km. The pressure and temperature of the tropopause as computed by the two methods is shown in Figure S3 in Supporting Information S1.

radiative effects are dominated by water vapor, whereas CO_2 concentrations are taken to extreme values in these simulations.

Four key changes are occurring simultaneously in our simulations: a slowdown of atmospheric circulation (weaker streamfunction, see Figure 2g–2i), an increase in the tropopause height, an increase in the moist component of atmospheric energy transport in the extratropics, and a moistening of the subtropics. The increase in tropopause height is expected as the surface temperature increases (Hu & Vallis, 2019; Seeley et al., 2019). The general slowdown of the circulation may be attributed to an increase in the moist contribution to the overall

energy transport, thus requiring a weaker overall circulation. Given a weaker circulation (and less intense Hadley Cell) a moistening of the subtropics can be expected (Pierrehumbert et al., 2007; Vallis, 2017). However, a fuller and more quantitative exploration of these effects requires future study.

4. Role of Relative Humidity Distribution Change

We now seek to understand the role of relative humidity change in the ECS peak. The forcing, feedback, and temperature change are related by: $F + \lambda \Delta T_S = 0$, where F is the top-of-atmosphere forcing (namely, the instantaneous change in the top-of-atmosphere radiative balance), ΔT_S is the change in surface temperature, and λ is (to use the conventional term) the feedback. The feedback (λ) can be calculated as the difference in top-of-atmosphere radiation of two simulations: one with fixed control surface temperature and one with the surface temperature increased by one degree from the control. When calculated in this way, the atmospheric temperature and specific humidity are allowed to increase and thus affect the TOA radiation budget. In order to isolate the effects of changes in relative humidity on the feedback, we calculate the feedback in a different but equivalent manner.

Between two equilibrated climates with CO_2 levels i and $i + 1$, the top-of-atmosphere forcing F is balanced by changes in the outgoing longwave radiation (OLR) and top-of-atmosphere net shortwave radiation (SW) such that $F + \Delta SW + \Delta OLR = 0$. The change in OLR can then separated into changes caused by surface temperature, atmospheric temperature, and specific humidity such that:

$$\underbrace{F + \Delta SW + \Delta OLR|_{\delta T_S \text{ and } T_a, SH \text{ fixed}} + \Delta OLR|_{\delta T_a \text{ and } T_S, SH \text{ fixed}} + \Delta OLR|_{\delta SH \text{ and } T_S, T_a \text{ fixed}}}_{\lambda \Delta T_S} = 0, \tag{1}$$

where ΔSW is the change in net shortwave radiation at the TOA between two successive simulations. And, in order to calculate the forcing F and the contributions to the change in OLR, the radiation code of the model is re-run in three dimensions with the time-mean patterns of T_s, T_a, and SH of the equilibrated climates with CO_2 levels i and $i + 1$, where c_i refers to the CO_2 concentration, as follows:

- $F = OLR(T_{S,i}, T_{a,i}, SH_i, c_{i+1}) - OLR(T_{S,i}, T_{a,i}, SH_i, c_i)$
- $\Delta OLR|_{\delta T_S \text{ and } T_a, SH \text{ fixed}} = OLR(T_{S,i+1}, T_{a,i}, SH_i, c_i) - OLR(T_{S,i}, T_{a,i}, SH_i, c_i)$
- $\Delta OLR|_{\delta T_a \text{ and } T_S, SH \text{ fixed}} = OLR(T_{S,i}, T_{a,i+1}, SH_i, c_i) - OLR(T_{S,i}, T_{a,i}, SH_i, c_i)$
- $\Delta OLR|_{\delta SH \text{ and } T_S, T_a \text{ fixed}} = OLR(T_{S,i}, T_{a,i}, SH_{i+1}, c_i) - OLR(T_{S,i}, T_{a,i}, SH_i, c_i)$

The forcing F is calculated such that we neglect the rapid adjustments which are often included in forcing estimates. The global mean of each of these terms is shown in Figure 3a for all simulations. The feedback, λ, is then decomposed into its SW component (λ_{SW}), and its longwave component is itself decomposed into its surface temperature contribution $\left(\lambda_{T_S}\right)$, its atmospheric temperature contribution $\left(\lambda_{T_a}\right)$, and its specific humidity component (λ_{SH}):

$$\lambda = \lambda_{SW} + \lambda_{T_S} + \lambda_{T_a} + \lambda_{SH}$$

with $\lambda_{SW} = \Delta SW/\Delta T_S$, $\lambda_{T_S} = \Delta OLR|_{\delta T_S \text{ and } T_a, SH \text{ fixed}}/\Delta T_S$, $\lambda_{T_a} = \Delta OLR|_{\delta T_a \text{ and } T_S, SH \text{ fixed}}/\Delta T_S$, and $\lambda_{SH} = \Delta OLR|_{\delta SH \text{ and } T_S, T_a \text{ fixed}}/\Delta T_S$.

$$\lambda = \left(\Delta SW + \Delta OLR|_{\delta T_S \text{ and } T_a, SH \text{ fixed}} + \Delta OLR|_{\delta T_a \text{ and } T_S, SH \text{ fixed}} + \Delta OLR|_{\delta SH \text{ and } T_S, T_a \text{ fixed}}\right)/\Delta T_S. \tag{2}$$

The feedback calculated as $F/\Delta T_S$ is shown in Figure 3b (black) and is compared to the feedback calculated as shown in Equation 2 (blue).

To estimate the impact of changes in relative humidity on the feedback, we recalculate the specific humidity component of the longwave feedback, as

$$\left(OLR\left(T_{S,i}, T_{a,i}, SH_{i+1} * \frac{RH_{300\text{ppm}}}{RH_{i+1}}, c_i\right) - OLR\left(T_{S,i}, T_{a,i}, SH_i * \frac{RH_{300\text{ppm}}}{RH_i}, c_i\right)\right)/\Delta T_S$$

where $RH_{300\text{ppm}}$ is the relative humidity for the 300 ppm simulation and RH_i is the relative humidity of the simulation at CO_2 level i. $SH_i * \frac{RH_{300\text{ppm}}}{RH_i}$ is equivalent to $SH_i^* * RH_{300\text{ppm}}$ where SH_i^* is the saturation specific humidity at CO_2 level i. Thus, this lets us estimate what the specific humidity would be if the relative humidity

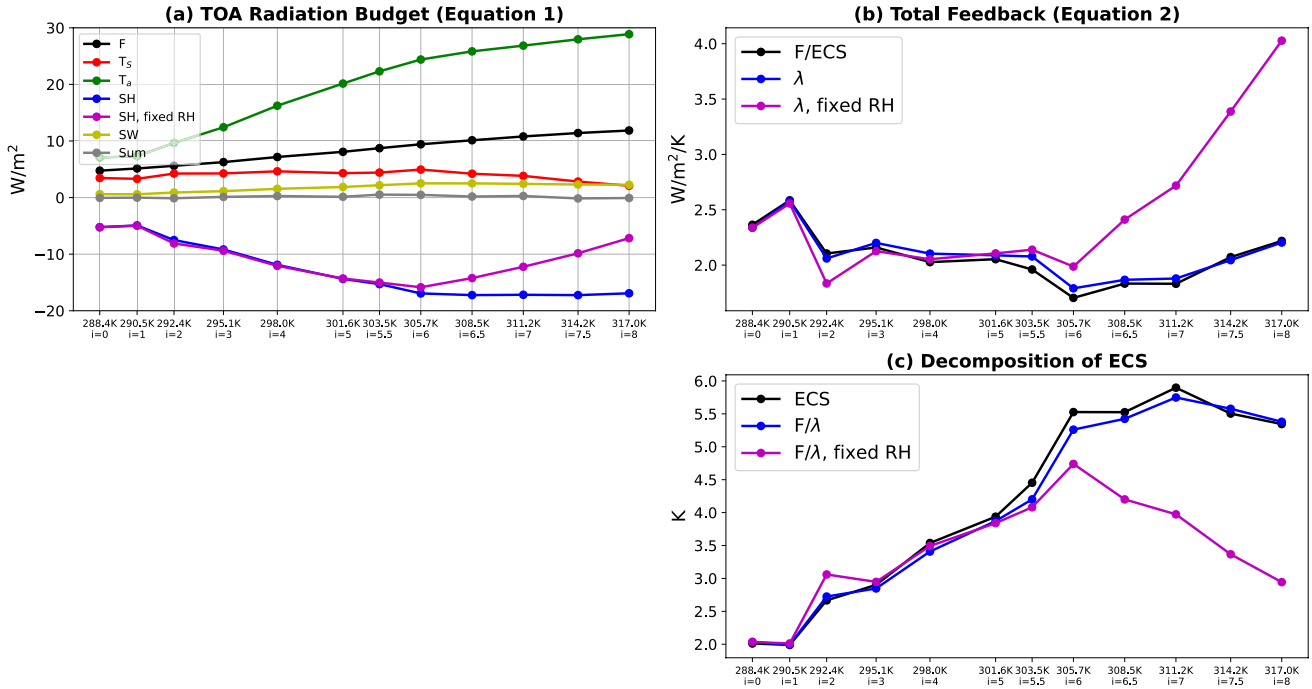

Figure 3. (a) TOA budget terms from Equation 1. The forcing F is calculated as the change in outgoing longwave radiation when CO_2 is increased while keeping T_S, T_a, and SH fixed. The "Ts" term is $\Delta OLR|_{\delta T_S \text{ and } T_a, SH \text{ fixed}}$, the "Ta" term is $\Delta OLR|_{\delta T_a \text{ and } T_S, SH \text{ fixed}}$, the "SH" term is $\Delta OLR|_{\delta SH \text{ and } T_S, T_a \text{ fixed}}$, the "SH, fixed RH" term is $\Delta OLR|_{\delta SH_i\ (RH_{300\text{ppm}}/RH_i), \text{and } T_S, T_a \text{ fixed}}$, the "SW" term is the change in net shortwave radiation at the TOA between two successive simulations, and the "Sum" term is the sum of all terms except the "SH, fixed RH" term. (b) The forcing (F) divided by the equilibrium climate sensitivity (ECS) (black), the total feedback (λ) as computed using Equation 2 (blue), and the total feedback with the assumption of fixed relative humidity (magenta). (c) The ECS (black), the forcing (F) divided by the total feedback (λ) (blue), and the same but with the feedback recalculated with the assumption of fixed relative humidity (magenta).

was held constant to its 300 ppm values. The impact of this change on the TOA response is shown in Figure 3a (magenta) and shows a weaker water vapor feedback for the high CO_2 simulations, which is reflected in the feedback (Figure 3b) and the ECS (Figure 3c).

The picture that emerges from the simulations is one in which a slowdown in atmospheric circulation causes a moistening of the subtropics, which radiate less efficiently to space (Pierrehumbert, 1995). This then increases the water vapor feedback and climate sensitivity at high CO_2 levels. Ignoring this moistening, and calculating the ECS assuming a fixed relative humidity (magenta in Figure 3c) results in a sharper peak at $i = 6$, which is more consistent with single column model simulations with comprehensive radiation and fixed relative humidity (Kluft et al., 2021; Seeley & Jeevanjee, 2021).

5. Latitudinal Decomposition of Changes in Relative Humidity and Feedback

In order to verify our hypothesis that the higher ECS (relative to the fixed relative-humidity ECS) for levels of CO_2 larger than 300 ppm $\times 2^6$ is caused by the moistening of the subtropics, we decompose the change in relative humidity and the terms of Equation 1 according to their latitude. Figure 4 shows the vertical structure of relative humidity between 0 and 40 degrees North (a) and between 40 and 90 degrees North (c), and the corresponding terms of Equation 1 (b, d). The averaged tropics and subtropics see a clear increase in relative humidity from around 40% to around 65% (Figure 4a), whereas there is only a modest decrease in relative humidity poleward of 40 degrees North (Figure 4c). The effect on the feedback can be deduced from the difference between the water vapor feedback term (SH, in blue) in Equation 1 and the fixed relative humidity water vapor feedback term (SH, fixed RH, in magenta). In the tropics and subtropics, the moistening of the atmospheric column increases the water vapor feedback (blue) compared to an atmosphere with fixed relative humidity (magenta) (Figure 4b), whereas in the region poleward of 40 degrees North, the water vapor feedback does not change when the relative humidity is fixed (Figure 4d).

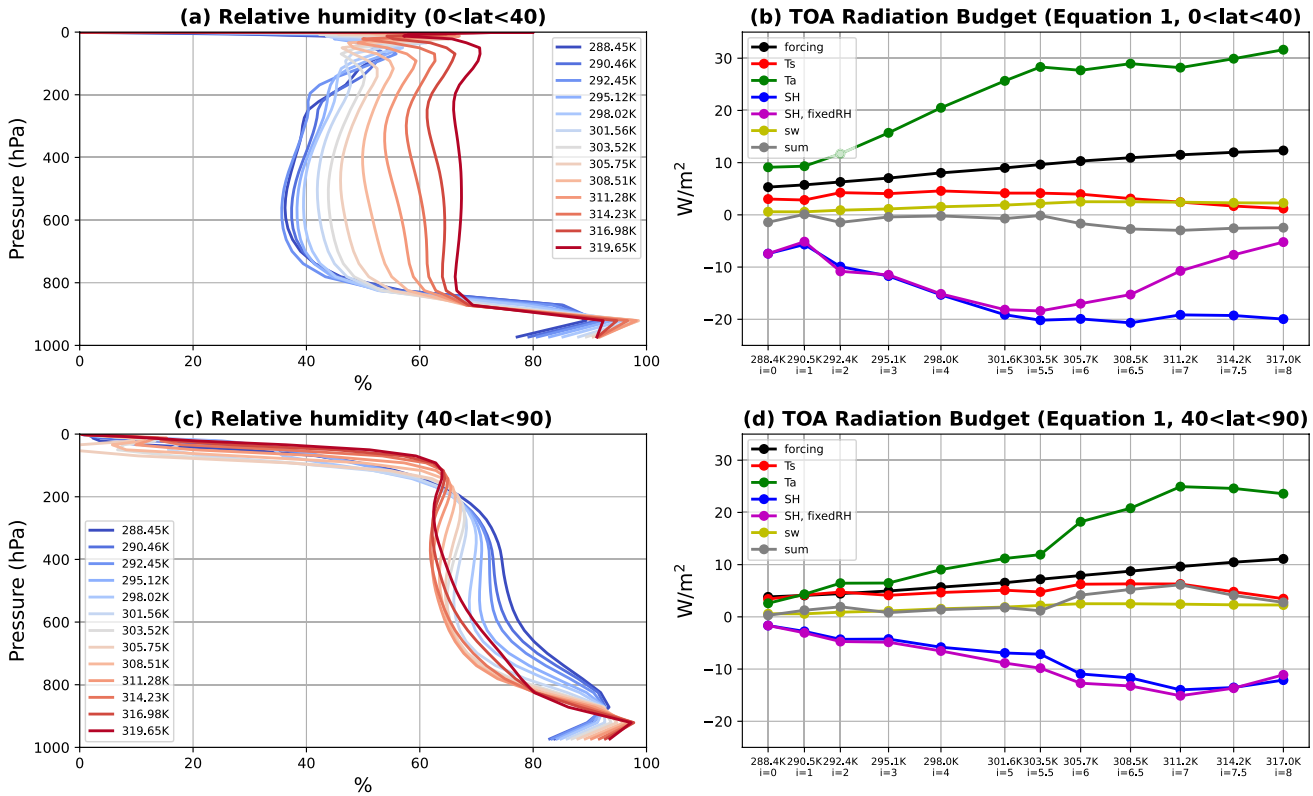

Figure 4. Vertical structure of changes in relative humidity (a, c) and TOA budget terms from Equation 1 (b, d) for latitudes in [0, 40] (a, b) and poleward of 40 degrees (c, d).

6. Summary and Conclusions

A peak in ECS has previously been found at around 310 K in a variety of climate models ranging from a single column model (Kluft et al., 2021; Seeley & Jeevanjee, 2021) to comprehensive climate models (e.g., Wolf & Toon, 2015). The purpose of this paper is to better understand the mechanisms and generality of these results by bridging the gap between the simple clear-sky explanation for the peak in ECS found in single column models and the complicated mechanisms present in comprehensive climate models. Among other things this allows us to look at variations in relative humidity, known to be important factor in determining the clear-sky longwave feedback (Bourdin et al., 2021; Zhang et al., 2020). To this end we use a clear-sky aquaplanet configuration of the Isca climate modeling framework (Vallis et al., 2018) with no sea ice, a slab ocean boundary condition, no clouds, annual-mean insolation, and a radiation scheme for infrared radiation which maintains good accuracy for CO_2 levels up 100,000 ppm and temperatures up to 500 K. As we increase CO_2 from 300 ppm (at 285.4 K) to $\approx$ 110,000 ppm (at 317.8 K), we find that the ECS plateaus around 310 K, with only a mild peak.

The reason for the lack of a sharp peak is that the tropical circulation weakens at very high temperatures, leading to a substantial moistening of the subtropics. To isolate the impact of this change in relative humidity on the longwave feedback, we decompose the change in OLR into changes caused by surface temperature, atmospheric temperature, and specific humidity. We then recalculate the feedback assuming no change in relative humidity, and in that case we do find a peak in ECS around 310 K, which is consistent with single column model results (Kluft et al., 2021; Seeley & Jeevanjee, 2021). We then confirm that it is the moistening of the subtropics which causes the increase in ECS by decomposing the feedback and relative humidity by latitude. Evidently, changes in the relative humidity, caused by changes in the circulation, need to be considered in any quantitative theory of climate sensitivity (as discussed e.g., in Bourdin et al. (2021)).

Data Availability Statement

The code to reproduce the figures is available at Henry (2023b) and the data is available at Henry (2023a). For the purpose of open access, the author has applied a Creative Commons Attribution (CC BY) licence to any Author Accepted Manuscript version arising.

Acknowledgments
We wish to thank all the Isca team for many discussions about climate science and modelling, and Nadir Jeevanjee for fruitful discussions about radiation. We also wish to thank Neil Lewis for the single column model code and James Manners for his help with the radiation code. Finally, we wish to thank the reviewers for very helpful comments. MH and GV were supported by NERC grant number NE/T00942X/1, under a NERC-NSF partnership "Dynamics of Warm Past and Future Climates." N.J.L was supported by the NOAA Climate Program Office's Modeling, Analysis, Predictions, and Projections program through grant NA20OAR4310387.

References

Anagnostou, E., John, E. H., Babila, T., Sexton, P., Ridgwell, A., Lunt, D. J., et al. (2020). Proxy evidence for state-dependence of climate sensitivity in the Eocene greenhouse. *Nature Communications*, *11*(1), 1–9. https://doi.org/10.1038/s41467-020-17887-x

Bloch-Johnson, J., Rugenstein, M., Stolpe, M. B., Rohrschneider, T., Zheng, Y., & Gregory, J. M. (2021). Climate sensitivity increases under higher CO_2 levels due to feedback temperature dependence. *Geophysical Research Letters*, *48*(4), e2020GL089074. https://doi.org/10.1029/2020gl089074

Bourdin, S., Kluft, L., & Stevens, B. (2021). Dependence of climate sensitivity on the given distribution of relative humidity. *Geophysical Research Letters*, *48*(8), e2021GL092462. https://doi.org/10.1029/2021gl092462

Frierson, D. M. (2007). The dynamics of idealized convection schemes and their effect on the zonally averaged tropical circulation. *Journal of the Atmospheric Sciences*, *64*(6), 1959–1976. https://doi.org/10.1175/jas3935.1

Henry, M. (2023a). Dataset for "State-dependence of the equilibrium climate sensitivity in a clear-sky GCM" by Matthew Henry et al. (2023) [Dataset]. Zenodo. https://doi.org/10.5281/zenodo.7892332

Henry, M. (2023b). matthewjhenry/ECS peak paper: Code for "State-dependence of the equilibrium climate sensitivity in a clear-sky GCM" by Henry et al. (2023) [Software]. Zenodo. https://doi.org/10.5281/zenodo.7892355

Hu, S., & Vallis, G. K. (2019). Meridional structure and future changes of tropopause height and temperature. *Quarterly Journal of the Royal Meteorological Society*, *145*(723), 1–20. https://doi.org/10.1002/qj.3587

Kluft, L., Dacie, S., Brath, M., Buehler, S. A., & Stevens, B. (2021). Temperature-dependence of the clear-sky feedback in radiative-convective equilibrium. *Geophysical Research Letters*, *48*(22), e2021GL094649. https://doi.org/10.1029/2021gl094649

Koll, D. D., & Cronin, T. W. (2018). Earth's outgoing longwave radiation linear due to H2O greenhouse effect. *Proceedings of the National Academy of Sciences*, *115*(41), 10293–10298. https://doi.org/10.1073/pnas.1809868115

Koll, D. D., Jeevanjee, N., & Lutsko, N. J. (2023). An analytic model for the clear-sky longwave feedback. *Journal of the Atmospheric Sciences*, *80*(8), 1923–1951. https://doi.org/10.1175/jas-d-22-0178.1

Leconte, J., Forget, F., Charnay, B., Wordsworth, R., & Pottier, A. (2013). Increased insolation threshold for runaway greenhouse processes on earth-like planets. *Nature*, *504*(7479), 268–271. https://doi.org/10.1038/nature12827

Manners, J., Edwards, J. M., Hill, P., & Thelen, J.-C. (2017). *SOCRATES: Suite of community RAdiative transfer codes based on Edwards and Slingo (technical report)*. UK Met Office.

Meraner, K., Mauritsen, T., & Voigt, A. (2013). Robust increase in equilibrium climate sensitivity under global warming. *Geophysical Research Letters*, *40*(22), 5944–5948. https://doi.org/10.1002/2013gl058118

Pierrehumbert, R. T. (1995). Thermostats, radiator fins, and the local runaway greenhouse. *Journal of the Atmospheric Sciences*, *52*(10), 1784–1806. https://doi.org/10.1175/1520-0469(1995)052<1784:trfatl>2.0.co;2

Pierrehumbert, R. T., Brogniez, H., & Roca, R. (2007). On the relative humidity of the atmosphere. In *The global circulation of the atmosphere* (Vol. 143, p. 185).

Popp, M., Schmidt, H., & Marotzke, J. (2016). Transition to a moist greenhouse with CO2 and solar forcing. *Nature Communications*, *7*(1), 1–10. https://doi.org/10.1038/ncomms10627

Romps, D. M. (2020). Climate sensitivity and the direct effect of carbon dioxide in a limited-area cloud-resolving model. *Journal of Climate*, *33*(9), 3413–3429. https://doi.org/10.1175/jcli-d-19-0682.1

Russell, G. L., Lacis, A. A., Rind, D. H., Colose, C., & Opstbaum, R. F. (2013). Fast atmosphere-ocean model runs with large changes in CO2. *Geophysical Research Letters*, *40*(21), 5787–5792. https://doi.org/10.1002/2013gl056755

Seeley, J. T., & Jeevanjee, N. (2021). H_2O windows and CO_2 radiator fins: A clear-sky explanation for the peak in equilibrium climate sensitivity. *Geophysical Research Letters*, *48*(4), e2020GL089609. https://doi.org/10.1029/2020gl089609

Seeley, J. T., Jeevanjee, N., & Romps, D. M. (2019). Fat or fitt: Are anvil clouds or the tropopause temperature invariant? *Geophysical Research Letters*, *46*(3), 1842–1850. https://doi.org/10.1029/2018gl080096

Thomson, S. I., & Vallis, G. K. (2019). The effects of gravity on the climate and circulation of a terrestrial planet. *Quarterly Journal of the Royal Meteorological Society*, *145*(723), 2627–2640. https://doi.org/10.1002/qj.3582

Vallis, G. K. (2017). *Atmospheric and oceanic fluid dynamics* (2nd ed.). Cambridge University Press.

Vallis, G. K., Colyer, G., Geen, R., Gerber, E., Jucker, M., Maher, P., et al. (2018). Isca, v1.0: A framework for the global modelling of the atmospheres of earth and other planets at varying levels of complexity. *Geoscientific Model Development*, *11*(3), 843–859. https://doi.org/10.5194/gmd-11-843-2018

Wolf, E., Haqq-Misra, J., & Toon, O. (2018). Evaluating climate sensitivity to CO_2 across earth's history. *Journal of Geophysical Research: Atmospheres*, *123*(21), 11–861. https://doi.org/10.1029/2018jd029262

Wolf, E., & Toon, O. (2015). The evolution of habitable climates under the brightening sun. *Journal of Geophysical Research: Atmospheres*, *120*(12), 5775–5794. https://doi.org/10.1002/2015jd023302

Zhang, Y., Jeevanjee, N., & Fueglistaler, S. (2020). Linearity of outgoing longwave radiation: From an atmospheric column to global climate models. *Geophysical Research Letters*, *47*(17), e2020GL089235. https://doi.org/10.1029/2020gl089235